Appl Biochem Biotechnol (2009) 155:330–346
DOI 10.1007/s12010-008-8397-7

β-D-Xylosidase from *Selenomonas ruminantium*: Thermodynamics of Enzyme-Catalyzed and Noncatalyzed Reactions

Douglas B. Jordan · Jay D. Braker

Received: 11 May 2008 / Accepted: 6 October 2008 /
Published online: 25 October 2008

Abstract β-D-Xylosidase/α-L-arabinofuranosidase from *Selenomonas ruminantium* is the most active enzyme known for catalyzing hydrolysis of 1,4-β-D-xylooligosaccharides to D-xylose. Temperature dependence for hydrolysis of 4-nitrophenyl-β-D-xylopyranoside (4NPX), 4-nitrophenyl-α-L-arabinofuranoside (4NPA), and 1,4-β-D-xylobiose (X2) was determined on and off (k_{non}) the enzyme at pH 5.3, which lies in the pH-independent region for k_{cat} and k_{non}. Rate enhancements (k_{cat}/k_{non}) for 4NPX, 4NPA, and X2 are 4.3×10^{11}, 2.4×10^{9}, and 3.7×10^{12}, respectively, at 25 °C and increase with decreasing temperature. Relative parameters $k_{cat}^{4NPX}/k_{cat}^{4NPA}$, $k_{cat}^{4NPX}/k_{cat}^{X2}$, and $(k_{cat}/K_m)^{4NPX}/(k_{cat}/K_m)^{X2}$ increase and $(k_{cat}/K_m)^{4NPX}/(k_{cat}/K_m)^{4NPA}$, $(1/K_m)^{4NPX}/(1/K_m)^{4NPA}$, and $(1/K_m)^{4NPX}/(1/K_m)^{X2}$ decrease with increasing temperature.

Keywords Fuel ethanol · Glycoside hydrolase · GH43 · k_{non} · pH dependence · Temperature dependence · Activation energy

Introduction

β-D-Xylosidase/α-L-arabinofuranosidase from the ruminal, anaerobic, and nonxylanolytic bacterium *Selenomonas ruminantium* (SXA) is a member of glycoside hydrolase family 43 and structural clan F in the Carbohydrate Active Enzymes database (http://www.cazy.org/) [1–3]. The enzyme is the most potent catalyst known, to date, for promoting the hydrolysis of 1,4-β-D-xylooligosaccharides to D-xylose, displaying values for k_{cat} and k_{cat}/K_m that are at least tenfold greater than reported for other β-xylosidases [4, 5]. Its catalytic prowess [4, 5], good stability versus extremes of pH and temperature [6], and bifunctionality of β-

The mention of firm names or trade products does not imply that they are endorsed or recommended by the US Department of Agriculture over other firms or similar products not mentioned.

D. B. Jordan (✉) · J. D. Braker
Fermentation Biotechnology Research Unit, National Center for Agricultural Utilization Research, US Department of Agriculture, Agricultural Research Service, 1815 N. University Street, Peoria, IL 61604, USA
e-mail: douglas.jordan@ars.usda.gov

xylosidase (EC 3.2.1.37) and α-arabinofuranosidase (EC 3.2.1.55) activities [4, 7, 8] bode well for application of SXA in industrial processes where it could serve in the hydrolysis of herbaceous biomass (arabinoxylan fraction) to simple sugars for subsequent fermentation to fuel ethanol and other bioproducts [9–11].

The X-ray structure of SXA with its active site occupied by 1,3-bis[tris(hydroxymethyl) methylamino]propane (Bis–Tris propane) shows a homotetrameric protein with protomers comprising two domains: an N-terminal five-bladed β-propeller domain that contains the two-subsite funnel-shaped active site, which has a single route for access by ligands; and a C-terminal β-sandwich domain that serves to restrict the size of the active site [12]. Structure-function studies have established that the SXA homotetramer dissociates to homodimers (K_d=70 nM) and the two quaternary states of SXA share quite similar values for steady-state kinetic parameters k_{cat} and k_{cat}/K_m [12]. SXA catalyzes hydrolysis of substrates with inversion of anomeric stereochemistry, implicating a single transition state with the catalytic base (D14, pK_a 5.0) serving to activate a water molecule for addition to substrate and the catalytic acid (E186, pK_a 7.2) serving to protonate the leaving group [4]. SXA catalyzes the hydrolysis of a single residue from the nonreducing end of substrate without processivity so that all products of the hydrolysis reaction are removed from the active site before initiating another catalytic cycle [4]. Monosaccharides can bind to the catalytically active, monoanionic form of SXA ($D14^{-}E186^{H}$) and the catalytically inactive, dianionic form of SXA ($D14^{-}E186^{-}$) but not to the diprotonated, catalytically inactive form of SXA ($D14^{H}E186^{H}$) [8]. Certain monosaccharides have been shown to bind twice to the $D14^{-}E186^{H}$ SXA, occupying subsites −1 and + 1, but only single binding of monosaccharides occurs with the $D14^{-}E186^{-}$ SXA [8]. Aminoalcohol inhibitors bind exclusively to subsite −1 where the amino group can interact with the anionic carboxyl group of E186 of the $D14^{-}E186^{-}$ form of SXA, and the aminoalcohol inhibitors can be used as probes to study the binding of monosaccharides and other ligands to subsite +1 [12].

β-D-Xylosidase and α-L-arabinofuranosidase activities share the single active site of the SXA protomer [4, 7, 8], and we have held continued interest in the action of SXA on substrates 4-nitrophenyl-β-D-xylopyranoside (4NPX), 4-nitrophenyl-α-L-arabinofuranoside (4NPA), and 1,4-β-D-xylooligosaccharides. In this work, we determined the influence of temperature on the steady-state kinetic parameters for SXA-catalyzed hydrolysis of 4NPX, 4NPA, and 1,4-β-D-xylobiose (X2) at pH 5.3 (Fig. 1) and compare them to the rates of hydrolysis off the enzyme (k_{non}). We show that viscosity of the reaction media has little influence on enzyme kinetic parameters for the three substrates so that k_{cat} and K_m can be considered as the rate constant for substrate to product conversion and the substrate binding constant, respectively, in the comparison. A method, accounting for side reactions of glycosides and monosaccharides (Fig. 2) that occur off the enzyme, was developed to provide more accurate rates for k_{non} for comparison with the enzyme rates.

Materials and Methods

Materials and General Methods

Buffers, 4-nitrophenol (4NP), 4NPX, 4NPA, L-arabinose (A1), and D-xylose (X1) were obtained from Sigma-Aldrich (St. Louis, MO, USA). X2 and D-xylose assay kit were from Megazyme (Wicklow, Ireland). β-Galactose dehydrogenase from *Pseudomonas fluorescens* was from Roche Applied Science (Indianapolis, IN, USA). Water was purified through a Milli-Q unit (Millipore; Billerica, MA, USA). All other reagents were of reagent grade and

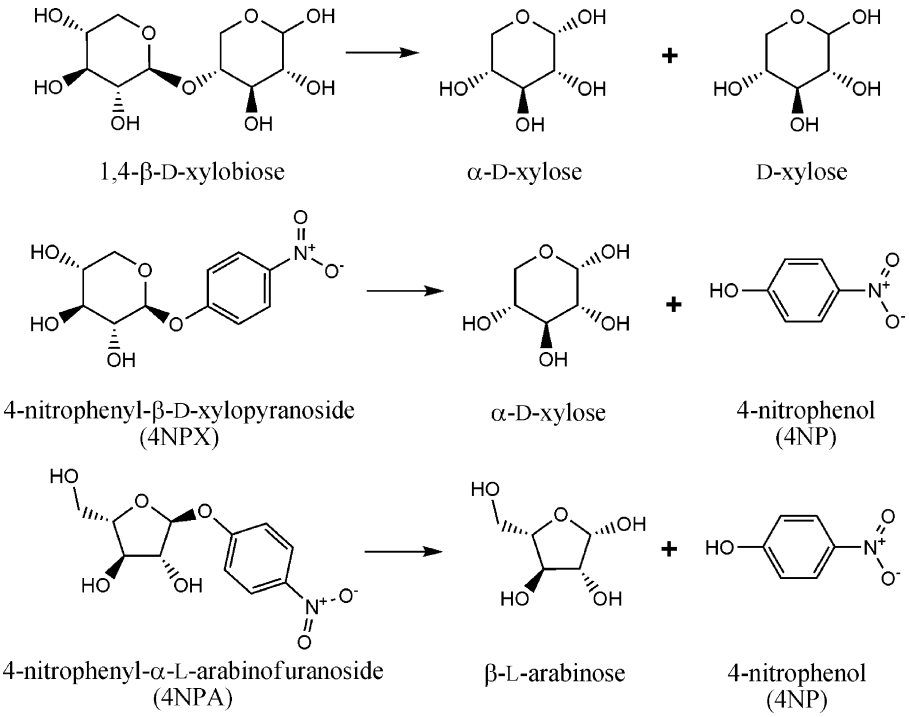

Fig. 1 Glycoside hydrolysis reactions studied on and off the enzyme. Initial products of the enzyme-catalyzed reactions are shown. The monosaccharide products isomerize off the enzyme (not shown)

high purity. Kinetic viscosity measurements were made at 25 °C using a Cannon-Fenske tube (Kimble); rates of sucrose solutions were divided by rates of water to yield relative viscosity (η/η_o). The gene encoding β-xylosidase from *S. ruminantium* GA192 was cloned and expressed in *Escherichia coli* as described [13]. SXA, produced in *E. coli*, was purified to homogeneity, as judged from the published sodium dodecyl sulfate polyacrylamide gel electrophoresis analysis [6], by using reverse-phase and anionic-exchange chromatography steps as described [4] with the addition of a final desalting, gel filtration step employing a 2.6×30-cm column of Bio-Gel P-6 DG desalting gel (Bio-Rad; Hercules, CA, USA), equilibrated and developed with 20 mM sodium phosphate, pH 7.3. Concentrations of homogeneous SXA protomers (active sites) were determined by using an extinction coefficient at 280 nm of 129,600 M^{-1} cm^{-1}, calculated from amino acid composition [4, 14]. A Cary 50 Bio UV-Visible spectrophotometer (Varian; Palo Alto, CA, USA), equipped

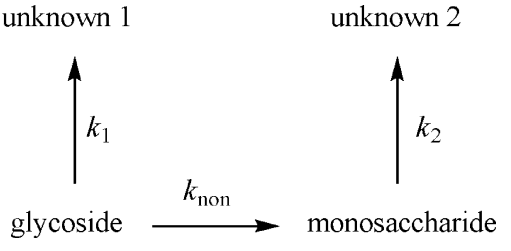

Fig. 2 Kinetic scheme for glycoside hydrolysis reactions and side reactions that occur off the enzyme. Rates of glycoside side reactions (k_1), concentrations of monosaccharides, and degradation rates of monosaccharides (k_2) were used to correct rates of glycoside loss ($k_{obs}=k_1+k_{obs}$) to provide rates of glycoside hydrolysis (k_{non})

with a thermostatted holder for cuvettes, was used for spectral and kinetic determinations. Kinetic simulations were through the computer program KINSIM: Chemical Kinetics Simulation System, 32-bit DOS-Extended Version 4.0, March 1997 [15]. The concentration of 4NP was determined by using the published extinction coefficient of 18.3 mM^{-1} cm^{-1} at 400 nm for 4NP in NaOH [16]. Concentrations of substrates 4NPX and 4NPA were determined by incubating substrate with excess enzyme until an end point was reached, adding an aliquot (10–100 μL) to 0.99–0.90 mL 0.1 M NaOH (for 4NPX) or 0.1 M sodium carbonate (for 4NPA), recording the absorbance at 400 nm and using the extinction coefficient of 18.3 mM^{-1} cm^{-1} for 4NP in NaOH. Concentrations of substrate X2 were determined by end point analysis, incubating an aliquot in 100 mM sodium succinate, pH 5.3, with excess SXA followed by analysis for D-xylose by high-performance liquid chromatography (HPLC) as described in the next section.

Hydrolysis of Substrates at Varied pH and Temperature off the Enzyme

Reactions (1.00 mL) contained substrates 4NPA (0.2 mM), 4NPX (0.2 or 1.0 mM), X2 (0.1 or 0.2 mM), D-xylose (0.1 or 0.2 mM), or L-arabinose (0.2 mM). Reactions were incubated in 4-mL glass vials maintained at constant temperature (temperature-controlled and monitored oven) and pH. For temperature studies, the substrates were incubated in 100 mM sodium succinate, pH 5.3, at 80, 90, and 100 °C. For pH studies, the substrates were incubated at 90 °C in 100 mM sodium phosphate (pH 2.0, 3.0, 7.0, and 8.0), 100 mM sodium succinate (pH 4.0, pH 5.3, and pH 6.0), and 100 mM sodium carbonate (pH 9.0). Prior to placing the reaction vials in the temperature-equilibrated oven, the vials were tightly sealed with a Teflon-lined screw cap. Samples for the progress curves were removed from the oven at varied times until at least one half of substrate had been consumed over the incubation time course or 28 days had elapsed. Upon removal from the oven, sample vials were cooled and stored at −20 °C until analyzed for substrates and products.

For the analyses, vials were thawed at room temperature and the reaction volumes were measured by using calibrated pipettes to account for loss of volume through evaporation. Volume losses were generally small and <17% in all cases. Postincubation volumes of reaction mixtures averaged 0.988±0.023 mL. Volume losses were used to correct concentrations of substrates and products, determined for each vial, by assuming that the volume loss was due to evaporation of water without loss of solutes: thus, the determined concentrations of substrates and products were multiplied by the volume of reaction mixtures (in milliliter) to arrive at the corrected concentrations. X2 reactions were analyzed for concentrations of X2 and D-xylose versus time. 4NPX reactions were analyzed for 4NPX and D-xylose versus time. 4NPA reactions were analyzed for 4NPA and L-arabinose versus time.

Concentrations of D-xylose and X2 in reactions were quantified by using a DX500 HPLC system equipped with an ED40 electrochemical detector (pulsed amperometry), AS3500 autosampler, PA-100 (4×250 mm) anion-exchange column, and Chromeleon software (Dionex Corp.; Sunnyvale, CA, USA). Samples (25 μL) were injected onto the column equilibrated with 0.1 M NaOH and developed with a 5-min linear gradient (0.1 M NaOH to 33 mM sodium acetate in 0.1 M NaOH) at ~25°C and a flow rate of 1 mL min^{-1}. Several concentrations of D-xylose and X2 were used to establish standard curves, on the same day that experimental samples were run.

Concentrations of 4NPA and 4NPX were determined by end point analysis using SXA. When necessary, aliquots (0.02–0.1 mL) of reaction mixtures in 1.0-cm path-length cuvettes were adjusted to pH 5–7 by adding a small volume (<0.1 mL) of neutralizing

solution (containing HCl or NaOH). Equivalent samples were treated or untreated to the addition of 7 μL SXA (0.3-mM active sites in 20 mM sodium phosphate, pH 7.3). Following 5-min incubations at ~25°C, solution volumes of cuvettes were brought to 1.0 mL by adding 100 mM sodium carbonate, pH 11 (for 4NPA analysis) or 100 mM NaOH (for 4NPX analysis). Absorbance of cuvettes at 400 nm was determined; the reading of the cuvettes untreated with SXA was subtracted from the reading of cuvettes treated with SXA, and the difference was divided by 18.3 mM^{-1} cm^{-1} to determine the concentration of 4NPA or 4NPX in the original sample.

Concentrations of L-arabinose were determined by end point analysis using β-galactose dehydrogenase. In a 1.0-cm path-length cuvette, an aliquot (200 μL) of incubated sample was adjusted to pH 9 by the addition of 100 μL NaOH solution. Addition of NAD^+ and sodium pyrophosphate solutions brought the cuvette volume to 993 μL. Absorbance of the cuvette was read at 340 nm prior to adding 0.7 units of β-galactose dehydrogenase in 7 μL, bringing the cuvette volume to 1.00 mL containing 1.0 mM NAD^+, 30 mM sodium pyrophosphate, pH 9.0. Reduction of NAD^+ to NADH was followed at 340 nm until end points of L-arabinose oxidation were reached (~20 min). Molar concentrations of L-arabinose were determined by dividing the absorbance changes at 340 nm by 6.3 mM^{-1} cm^{-1} [17, 18].

Determination of Rate Constants for Incubations off the Enzyme

Data for the loss of monosaccharide versus time were fitted to a first-order rate equation with a zero end point (Eq. 1). Thus, in accordance with the kinetic scheme of Fig. 2, k_{obs} of Eq. 1 equals k_2 (the degradation rate of monosaccharide to unidentified 2). Data for the loss of glycoside versus time were fitted to Eq. 1. In this case, k_{obs} of Eq. 1 equals the combined rates of k_{non} (glycoside bond cleavage) and k_1 (loss of glycoside to unidentified 1). To determine explicit values for k_{non} and k_1, concentrations of monosaccharide product during the reaction progression were determined. The concentration of the monosaccharide with time depends on the concentration of glycoside at time zero and rate constants for k_{non}, k_1, and k_2. Numerical calculations using the computer program KINSIM were used to arrive at approximations for the explicit values for k_{non} and k_1 that accurately predict the determined concentration of monosaccharide versus time. Thus, by using determined values for the glycoside concentration at time zero, the first-order rate constant k_2, and iteratively varied values for k_{non} and k_1 (keeping $k_{non}+k_1$ equal to k_{obs}, the first-order rate constant for loss of the glycoside) as inputs to KINSIM, the concentration of hydrolysis product (the monosaccharide) versus time can be approximated and explicit values for k_{non} and k_1 can be determined. Iterative variation in the values of k_{non} and k_1 continued until changes were <1% of k_{obs} ($k_{non}+k_1$) and the best values were selected by having the lowest sum of squared residuals (determined concentration of monosaccharide − fitted concentration for the monosaccharide)^2.

SXA-Catalyzed Reactions at Varied Temperatures and pH 5.3

For determination of steady-state kinetic parameters for SXA-catalyzed hydrolysis of X2, 0.5-mL reaction mixtures contained varied substrate concentrations (0.43–9.6 mM) in 100 mM sodium succinate, pH 5.3 at 5.5, 15, 20, and 25 °C. Before (time=0 min) and after (time=0.5 and 1 min) initiating reactions with enzyme (7 μL SXA in 20 mM sodium phosphate, pH 7.3), 100-μL aliquots of reaction mixtures were removed and quenched with an equal volume of 0.2 M sodium phosphate ~pH 11.3 at 0 °C (so that quenched mixtures were pH 10.5–11) and diluted by adding 1 mM sodium phosphate, pH 10.5–11, at 0 °C as

necessary (typically 200–800 μL added to 200 μL quenched samples) to adjust product D-xylose concentrations to fall within the linear range of standard curves of D-xylose concentrations. Samples were kept on wet ice or the HPLC autosampler at 5 °C until analyzed for D-xylose produced by HPLC as described in the "Hydrolysis of Substrates at Varied pH and Temperature off the Enzyme" section. Initial rates, calculated from linear regressions of the [D-xylose] produced versus time, were fitted to Eq. 3 for determination of steady-state kinetic parameters. Parameter, k_{cat}, is expressed in moles of substrate hydrolyzed per second per mole enzyme active sites (protomers).

For determination of steady-state kinetic parameters of SXA-catalyzed hydrolysis of 4NPX, 1.0-mL reaction mixtures contained varied substrate concentrations (0.10–5.0 mM) in 100 mM sodium succinate, pH 5.3 at 5.5, 15, 19.8, 25.2, 30.8, 35.2, and 40.4 °C. After (time=0.3–20 min) initiating reactions with enzyme (7 μL SXA in 20 mM sodium phosphate, pH 7.3), 100-μL aliquots of reaction mixtures were removed and added to a 1-cm path-length cuvette containing 0.1 M NaOH and the absorbance was read at 400 nm. Absorbance versus time points (n=4–6) produced straight lines. The slopes were corrected for dilution, divided by 18.3 mM^{-1} cm^{-1} for 4NP absorbance in NaOH, and divided by the concentration of enzyme active sites to convert to millimolar substrate hydrolyzed per second per millimolar enzyme active sites, which were used as initial rates. Initial rates were fitted to Eq. 3 for the determination of steady-state kinetic parameters.

For the determination of steady-state kinetic parameters of SXA-catalyzed hydrolysis of 4NPA, 1.0-mL reaction mixtures contained varied substrate concentrations (0.20–5.1 mM) in 100 mM sodium succinate, pH 5.3 at 5.5, 15, 20.2, 25.2, 30.1, 35.1, and 39.9 °C. After (time=0.3–20 min) initiating reactions with enzyme (7 μL SXA in 20 mM sodium phosphate, pH 7.3), 100-μL aliquots of reaction mixtures were removed and added to a 1-cm path-length cuvette containing 0.1 M sodium carbonate and the absorbance was read at 400 nm. Absorbance versus time points (n=4–6) produced straight lines. The slopes were used to determine steady-state kinetic parameters as for 4NPX in the paragraph preceding this.

SXA-Catalyzed Hydrolysis of X2 at Varied Viscosities and pH 5.3

Reaction mixtures (0.5-mL) contained varied X2 concentrations (0.2–8.0 mM) in 100 mM sodium succinate, pH 5.3, at 25 °C and either 0% sucrose (relative viscosity=η/η_o=1.0) or 50% sucrose (w/v, η/η_o=6.4). Before (time=0 min) and after (time=1 min) initiating reactions with enzyme (7 μL SXA in 20 mM sodium phosphate, pH 7.3), 0.486 mL of modified quenching solution from the D-xylose assay kit, containing 280 mM triethanolamine, 20 mM $MgCl_2$, 0.0056% sodium azide, 7.3 mM NAD^+, and 91 mM ATP, pH 7.8, was added to each reaction mixture, bringing the final pH to 7.4. Triethanolamine is a strong competitive inhibitor of SXA: at pH 7.0 and 25°C, $K_i^{triethanolamine} = 0.1$ mM [19]. Quenched samples were mixed and incubated for 10 min with 7 μL containing seven units hexokinase from the D-xylose assay kit and the absorbance was read at 340 nm. Reactions were mixed and incubated for 6 min with 7 μL of a solution from the D-xylose assay kit containing 120 units per milliliter of β-D-xylose dehydrogenase and 4.1 mg/mL of D-xylose mutarotase. After 6 min, the samples were read at 340 nm. The 340-nm absorbance of the time zero reactions were subtracted from the time 1-min reactions; molar concentrations of D-xylose produced were determined by dividing the absorbance differences by 6.3 mM^{-1} cm^{-1} [17, 18]. Initial rates ([X2] hydrolyzed per second) were fitted to Eq. 3 for the determination of steady-state kinetic parameters.

Equations

Data were fitted to equations by using the computer program Grafit (Erithacus Software; Horley, UK) [20]. Symbol definitions for Eqs. 1–5: A is the concentration of substrate at time t; A_0 is the concentration of substrate at time zero; k_{obs} is the first-order rate constant; t is the time; k_H is the second-order rate constant for specific acid-catalyzed hydrolysis; α_H is the proton activity coefficient; k_{OH} is the second-order rate constant for specific base-catalyzed hydrolysis; K_W is the dissociation constant of water (3.82×10^{-13} at 90 °C) [21]; k_0 is the first-order rate constant for spontaneous hydrolysis; v is the observed initial (steady-state) rate of catalysis; k_{cat} is the maximum rate of catalysis; S is the substrate concentration; K_m is the Michaelis constant; $\Delta H°$ is the standard enthalpy change; R is the universal gas constant (1.987 cal mol^{-1} K^{-1}); T is the temperature in Kelvin; $\Delta S°$ is the standard entropy change; $\Delta H^{‡}$ is the activation enthalpy; $\Delta S^{‡}$ is the activation entropy; k_B is Boltzmann's constant (1.3807×10^{-23} J K^1); h is Planck's constant (6.626×10^{-34} J s); p is kinetic parameter k_{non}, k_{cat}, or k_{cat}/K_m; k_{non} is the hydrolysis rate off the enzyme, and K_{TX} is the dissociation constant of the transition state from the enzyme.

$$A = A_0 e^{-k_{obs}*t} \tag{1}$$

$$k_{obs} = k_H \times \alpha_H + k_{OH} \times \frac{K_W}{\alpha_H} + k_0 \tag{2}$$

$$v = \frac{k_{cat} \times S}{K_m + S} \tag{3}$$

$$\ln\frac{1}{K_m} = -\frac{\Delta H°}{R \times T} + \frac{\Delta S°}{R} \tag{4}$$

$$\ln\frac{p}{T} = -\frac{\Delta H^{‡}}{R \times T} + \frac{\Delta S^{‡}}{R} + \ln\frac{k_B}{h} \tag{5}$$

$$K_{TX} = k_{non} \times \frac{K_m}{k_{cat}} \tag{6}$$

Results and Discussion

Rates for the hydrolysis of glycosides off the enzyme (k_{non}) do not equate to the observed rates (k_{obs}) for glycoside consumption because, as indicated by the schematic of Fig. 2, loss of glycoside can occur by two routes, one yielding monosaccharide with associated rate constant k_{non} for the hydrolysis reaction and the other yielding product(s) (unidentified 1) with associated rate constant k_1. Thus, the determined rate for the loss of glycoside versus time (k_{obs}) is the combined rates of k_{non} and k_1. Values for k_{non} and k_1 can be resolved from

k_{obs} for the loss of glycoside by determining values for k_{obs} and k_2 and the concentration of monosaccharide product versus time followed by numerical fitting of the concentrations of product monosaccharide to the kinetic scheme of Fig. 2 using varied rates for k_{non} and k_1, keeping their sum equal to k_{obs} for the loss of the glycoside, until the concentrations of monosaccharide versus time are well matched. Fortunately, from individual incubations at all of the varied conditions of pH and temperature in this study, the loss of glycoside substrate with time (e.g., 4NPX) and the loss of its product monosaccharide (e.g., D-xylose) with time fit well to Eq. 1, which describes a first-order decay with zero end point (Fig. 3a). This makes the system tractable for solving the individual contributions of k_{non} and k_1 to k_{obs}. An example of k_{non} and k_1 resolution from k_{obs} is provided in Fig. 3b, which shows data for the concentration of D-xylose from the progress curve of an incubation of 1.04 mM 4NPX at 90 °C in 100 mM sodium succinate, pH 6.0. Using KINSIM inputs of 1.04 mM 4NPX as the initial concentration of glycoside, 1.73×10^{-4} min^{-1} for k_2, the rate constant determined for the loss of D-xylose versus time under the same conditions (Fig. 3a), and varied inputs for the rate constants k_{non} and k_1, keeping their sum equal to 6.60×10^{-5} min^{-1} for k_{obs}, the rate of 4NPX decay (Fig. 3a), the initial estimates for k_{non} and k_1 generated KINSIM simulations (indicated by the dotted curves of Fig. 3b) for the concentrations of D-xylose versus time that were refined iteratively until the k_{non} and k_1 values produced KINSIM simulations that closely match the observed concentrations of D-xylose versus

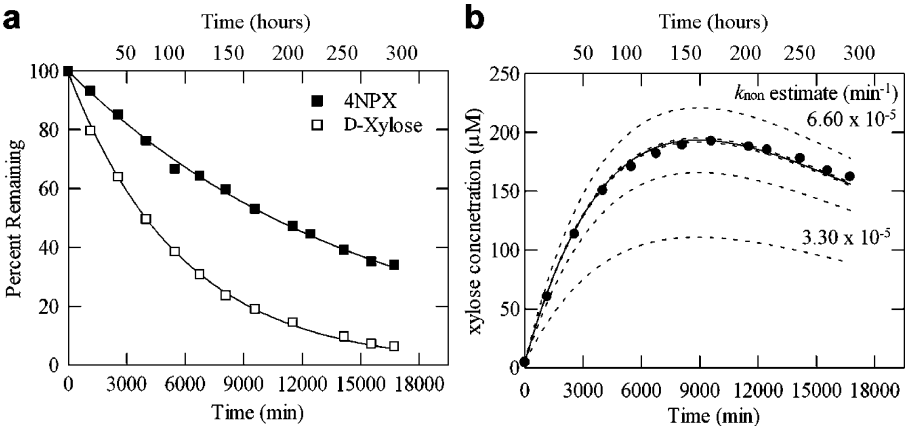

Fig. 3 Resolution of k_1 and k_{non} values from k_{obs}. **a** Decay curves for the loss of 4NPX and D-xylose versus time. 4NPX (1.04 mM) and D-xylose (0.204 mM) were incubated separately at 90 °C in 100 mM sodium succinate, pH 6.0. With time, samples were analyzed for the percent 4NPX remaining (*filled squares*) and the percent D-xylose remaining (*empty squares*). *Curves* were generated by fitting the data to Eq. 1: for 4NPX, $A_0 = 99.2 \pm 0.5\%$ and $k_{obs} = (6.60 \pm 0.09) \times 10^{-5}\,\text{min}^{-1}$; for D-xylose, A_0=99.9±0.6% and k_2=(1.73±0.02)×10^{-4} min^{-1}. **b** Simulation of the concentration of D-xylose produced from 4NPX versus time. Concentrations of D-xylose (*filled circles*) were determined from incubations containing 1.04 mM 4NPX in 100 mM sodium succinate, pH 6.0 at 90 °C. The D-xylose concentrations versus time plot was simulated using the kinetic scheme of Fig. 2 and the computer program KINSIM with the following inputs: initial 4NPX concentration=1.04 mM and the first-order rate constant for D-xylose decay from **a** = k_2=1.73×10^{-4} min^{-1}. KINSIM input values for k_1 and k_{non} were varied, keeping their sum equal to the first-order rate constant for 4NPX decay from **a** $\left(k_{non} + k_1 = k_{obs} = 6.60 \times 10^{-5}\,\text{min}^{-1}\right)$. For example, in the first approximation, k_{non} was set as 6.60×10^{-5} min^{-1} and k_1 was set as 0 min^{-1} as represented by the indicated *dotted curve*. The second iteration set k_{non}=k_1=3.30×10^{-5} min^{-1} as shown by the indicated *dotted curve*. Iterations continued until 5×10^{-7} min^{-1} (<1% of the k_{obs} value) changes in k_1 and k_{non} input values caused no improvement in the sum of squares of residuals (observed−simulated)^2. The best fit is indicated by the *solid curve*: k_{non}=(5.78±0.01)×10^{-5} min^{-1} and k_1=(8.2±0.1)×10^{-6} min^{-1}

time in the incubations. Iterations of k_{non} and k_1 values were continued until the simulated curves matched the D-xylose concentrations by visual inspection and changes in the estimates for k_{non} and k_1 by less than 1% of the k_{obs} rate produced no further minimization of the sum of squares of residuals, ∑(observed D-xylose concentration−KINSIM simulated D-xylose concentration)^2.

By using KINSIM resolutions of k_{obs}, rates of hydrolysis (k_{non}) for 4NPX, 4NPA, and 1,4-β-xylobiose were determined at varied pH (2–9) and 90 °C (Fig. 4). For comparison, unrefined k_{obs} values for the loss of glycoside versus time are plotted (hollow circles) with the refined k_{non} values (solid circles). As shown, differences between k_{non} and k_{obs} are larger at higher pH for X2 (and to a smaller extent 4NPX, but not 4NPA), suggesting that the difference ($k_{obs}-k_{non}=k_1$) is base-catalyzed. Monosaccharide (D-xylose and L-arabinose) decay (k_2) is also base-catalyzed (data not shown). In a study that used sodium phosphate as the buffer, the decay of monosaccharide was shown to be general-base-catalyzed [22]. Rates of hydrolysis (k_{non}) for the three glycoside substrates fit well to Eq. 2, which describes base-catalyzed, acid-catalyzed, and spontaneous rate dependencies. The flat-bottomed V-shaped pH patterns are similar to the reported pH dependencies of nitrophenyl

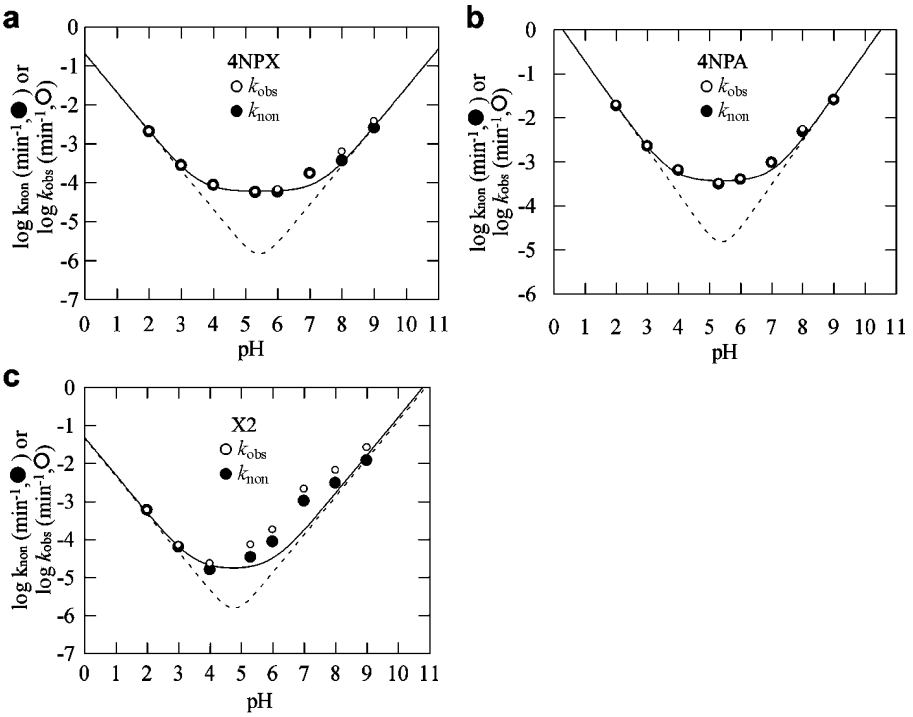

Fig. 4 Influence of pH on the rates (k_{non} values) of hydrolysis of glycosides off the enzyme. Glycosides were incubated at varied pH and 90 °C. Values for k_{non} (*filled circles*) were resolved from values for k_{obs} (*empty circles*) as described. For each reaction, *solid curves* were generated by fitting the k_{non} data to Eq. 2. *Dotted curves* were generated by using the fitted values for k_H and k_{OH} and setting k_0 to zero. **a** 4NPX. Fitted Eq. 2 parameters: $k_H=(2.06\pm0.36)\times10$ min^{-1}, $k_{OH}=7.29\pm1.20$ min^{-1}, and $k_0=(5.93\pm0.67)\times10^{-5}$ min^{-1}. Nadir of *dotted curve* at pH 5.4; rate=1.5×10^{-6} min^{-1}. **b** 4NPA. Fitted Eq. 2 parameters: $k_H=1.89\pm0.34$ min^{-1}, $k_{OH}=80.5\pm13.8$ min^{-1}, and $k_0=(3.55\pm0.54)\times10^{-4}$ min^{-1}. Nadir of *dotted curve* at pH 5.4; rate=1.5×10^{-5} min^{-1}. **c** 1,4-β-xylobiose. Fitted Eq. 2 parameters: $k_H=0.0491\pm0.0267$ min^{-1}, $k_{OH}=43.4\pm16.9$ min^{-1}, and $k_0=(1.61\pm0.89)\times10^{-5}$ min^{-1}. Nadir of *dotted curve* at pH 4.7; rate=1.8×10^{-6} min^{-1}

β-glucopyranosides [23], which established the involvement of specific-acid catalysis, specific-base catalysis, and spontaneous hydrolysis. The same study showed that rates of hydrolysis of nitrophenyl α-glucopyranosides have the specific-acid-catalyzed and the specific-base-catalyzed components but lack the spontaneous component, establishing that the spontaneous rate is due to the *trans*-1,2 orientation of the nitrophenoxy group and the C2–OH group of the nitrophenyl β-glucopyranosides, which provides the means for neighboring group participation by the C2–OH group in displacement of the nitrophenoxy group. Neighboring group participation is not available to the nitrophenyl α-glucopyranosides owing to their *cis*-1,2 dispositions. The *trans*-1,2 disposition of the C2–OH group and the aglycone is shared by 4NPX, 4NPA, and 1,4-β-xylobiose and provides means for intramolecular catalysis and the observed spontaneous rates (Fig. 4). As a visual aid, the dotted curves of Fig. 4, drawn from the fitted parameters except that the spontaneous rate constant (k_0) was set to zero, project the hydrolysis rates in the absence of spontaneous (neighboring group) catalysis for comparison with the solid curves, which were drawn from the complete fitted parameters.

Subtracting the spontaneous rate constant (k_0) from the k_{non} values at each pH of Fig. 4 shows that the spontaneous rates dominate specific-acid- and specific-base-catalyzed rates most at pH 5.4, pH 5.4, and pH 4.7 for 4NPX, 4NPA, and X2, respectively, and pH 5.3, within the pH-independent region, was chosen for studying the temperature dependencies for hydrolysis. k_{cat} values of SXA are pH independent between pH 4.5 and 6.0 for the three substrates [4, 5].

Previously, we showed that the steady-state kinetic parameters k_{cat} and k_{cat}/K_m for SXA acting on 4NPX and 4NPA at 25 °C were modestly (<12%) affected by the viscosity of the reaction media (comparing kinetic parameters determined at relative viscosities (η/η_o) of 1 and 6), strongly suggesting that substrate binding and product release steps are not rate limiting for these substrates in the enzyme-catalyzed reaction [4]. For this work, we determined the influence of viscosity on the steady-state parameters of SXA acting on X2. From SXA-catalyzed reactions at pH 5.3 and 25 °C, the ratios of kinetic parameters determined at high relative viscosity (50% sucrose (*w*/*v*), η/η_o=6.4) divided by the kinetic parameters determined at low relative viscosity (0% sucrose (*w*/*v*), η/η_o=1.0) are $(k_{cat})^{\eta/\eta o=6.4}/(k_{cat})^{\eta/\eta o=1} = 0.690 \pm 0.016$, $(k_{cat}/K_m)^{\eta/\eta o=6.4}/(k_{cat}/K_m)^{\eta/\eta o=1} = 0.883 \pm 0.045$, and $(K_m)^{\eta/\eta o=6.4}/(K_m)^{\eta/\eta o=1} = 0.783 \pm 0.054$. Had substrate binding and product release steps been fully limited by diffusion, the ratios of rate constants would have approached 0.156. Thus, the rate

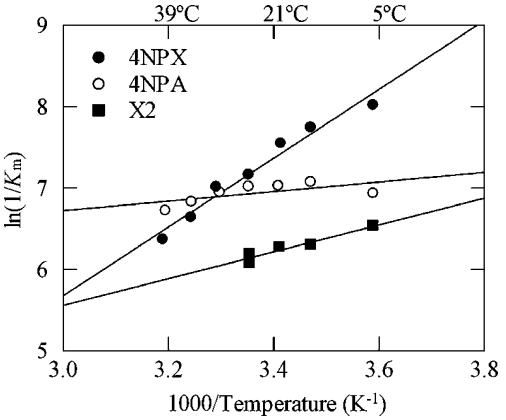

Fig. 5 van't Hoff plot ($1/K_m$ versus 1,000/Kelvin) for SXA substrates. Initial rates were determined from reactions containing 100 mM sodium succinate, pH 5.3, and varied substrate concentrations at temperatures 5.5 to 40.4 °C. The data were fitted to Eq. 3 to determine steady-state kinetic parameters. Values for $1/K_m$ and associated standard errors are plotted. *Curves* were generated by fitting $1/K_m$ data to the van't Hoff equation, Eq. 4

constants for SXA-catalyzed reactions, as determined in nonviscous medium, are weakly influenced by limiting rates for substrate binding or product release. It can be calculated that diffusion lowers the reported k_{cat} and k_{cat}/K_m for 4NPX and 4NPA by <2% at pH 5.3, 25 °C, and η/η_o of 1.0, whereas the corresponding values for X2 are lowered by 8% or less. Therefore, for SXA acting on 4NPX, 4NPA, and X2, K_m values can be considered as binding constants (K_s values) and k_{cat} values can be considered as rate constants for hydrolyzing the

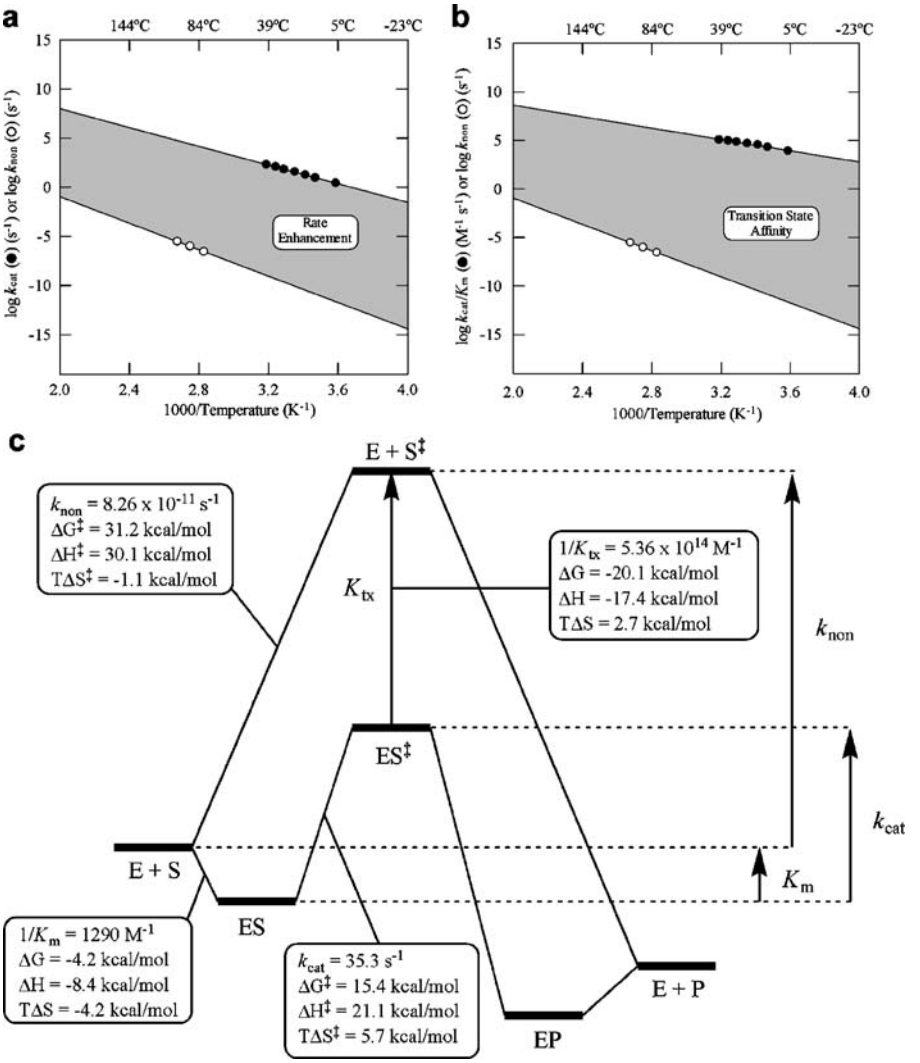

Fig. 6 Thermodynamics of 4NPX hydrolysis on and off the enzyme. Values for k_{non} were determined from incubations of 4NPX in 100 mM sodium succinate, pH 5.3, at 80, 90, and 100 °C. Steady-state kinetic parameters of SXA-catalyzed reactions were determined from reactions containing varied concentrations of 4NPX in 100 mM sodium succinate, pH 5.3 at 5.5, 15, 19.8, 25.2, 30.8, 35.2, and 40.4 °C. **a** Temperature dependence of k_{non} and k_{cat}. Kinetic parameters were fitted to the Eyring equation, Eq. 5. Fitted parameters are listed in Table 1. **b** Temperature dependence of k_{non} and k_{cat}/K_m. Kinetic parameters were fitted to the Eyring equation, Eq. 5. Fitted parameters are listed in Table 1. **c** Energy profile for the hydrolysis of 4NPX on and off the enzyme at 25 °C

glycosidic bond, which is important for accurate determination of K_{TX}, the dissociation constant of the transition state from the enzyme.

Temperature dependence of SXA-catalyzed hydrolysis of 4NPX, 4NPA, and X2 were determined at pH 5.3 and between 5.5 and 40.4 °C. The van't Hoff plots of $1/K_m$ versus 1,000/Kelvin are shown in Fig. 5. Eyring plots of k_{cat} and k_{cat}/K_m versus 1,000/Kelvin are in Figs. 6, 7, and 8. Hydrolysis rates (k_{non}) of the three glycosides off the enzyme were

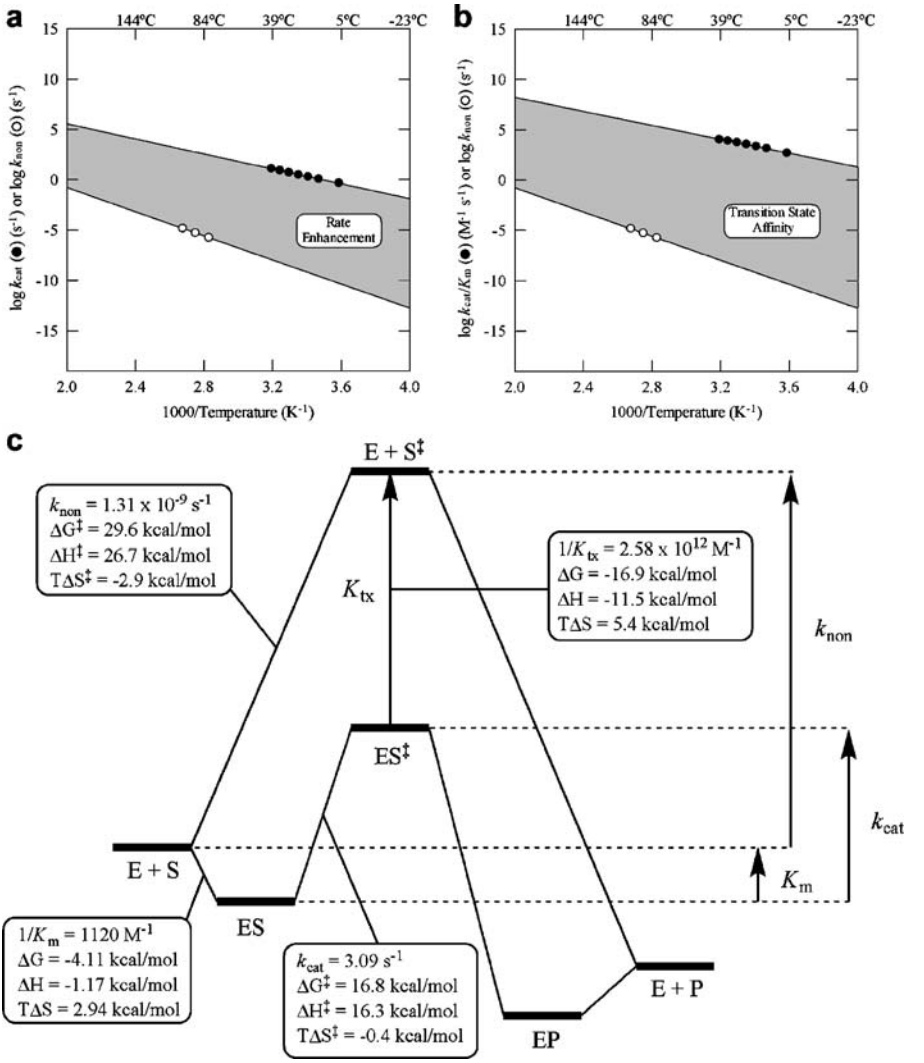

Fig. 7 Thermodynamics of 4NPA hydrolysis on and off the enzyme. Values for k_{non} were determined from incubations of 4NPA in 100 mM sodium succinate, pH 5.3, at 80, 90, and 100 °C. Steady-state kinetic parameters of SXA-catalyzed reactions were determined from reactions containing varied concentrations of 4NPA in 100 mM sodium succinate, pH 5.3 at 5.5, 15, 20.2, 25.2, 30.1, 35.1, and 39.9 °C. **a** Temperature dependence of k_{non} and k_{cat}. Kinetic parameters were fitted to the Eyring equation, Eq. 5. Fitted parameters are listed in Table 1. **b** Temperature dependence of k_{non} and k_{cat}/K_m. Kinetic parameters were fitted to the Eyring equation, Eq. 5. Fitted parameters are listed in Table 1. **c** Energy profile for the hydrolysis of 4NPA on and off the enzyme at 25 °C

determined at 80, 90, and 100 °C and pH 5.3, and the resulting Eyring plots of the k_{non} data are shown in Figs. 6, 7, and 8 for comparison with the enzyme kinetic parameters. All temperature-dependent parameters, corrected to 25 °C, are listed in Table 1. Free-energy profiles for the hydrolysis reactions on and off the enzyme are shown in Figs. 6, 7, and 8. Rate enhancement is the ratio k_{cat}/k_{non}, and transition-state affinity (K_{TX}) is determined from Eq. 6 or the relationship $K_{TX} = K_m \times k_{non}/k_{cat}$ [24].

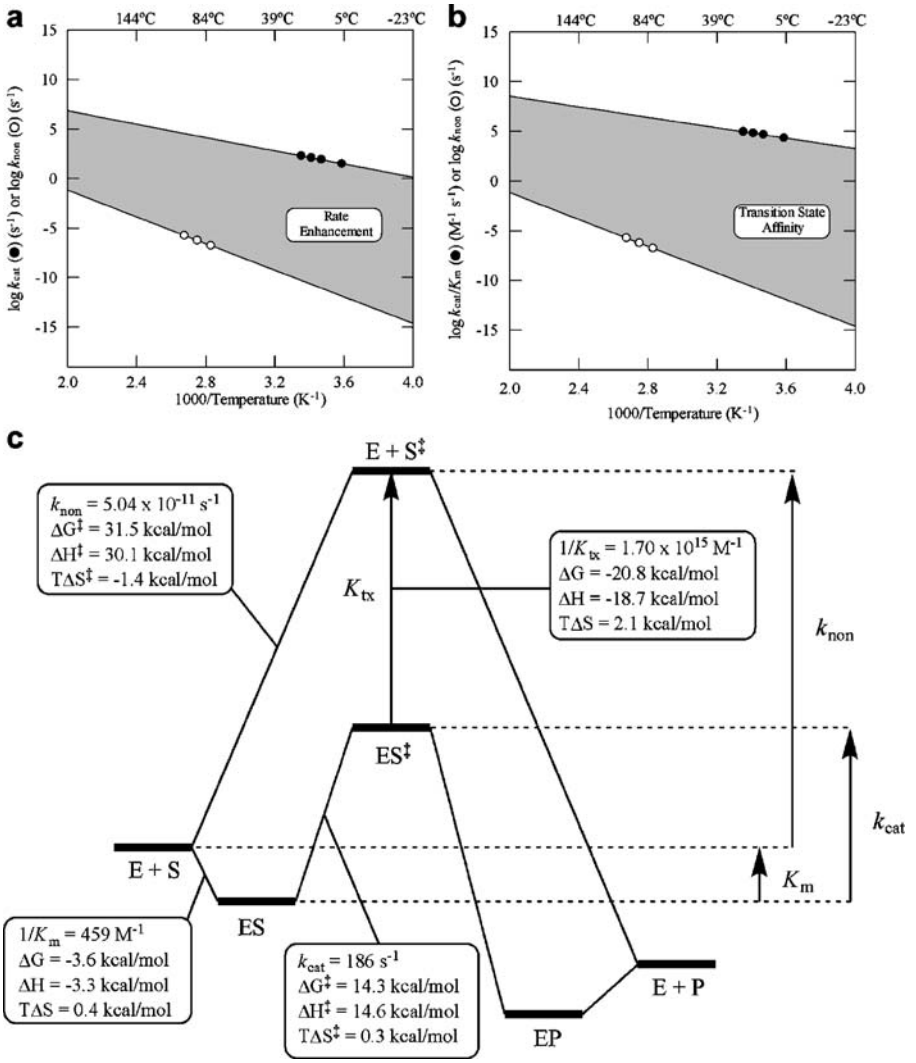

Fig. 8 Thermodynamics of 1,4-β-xylobiose hydrolysis on and off the enzyme. Values for k_{non} were determined from incubations of X2 in 100 mM sodium succinate, pH 5.3, at 80, 90, and 100 °C. Steady-state kinetic parameters of SXA-catalyzed reactions were determined from reactions containing varied concentrations of X2 in 100 mM sodium succinate, pH 5.3 at 5.5, 15, 20, and 25 °C. **a** Temperature dependence of k_{non} and k_{cat}. Kinetic parameters were fitted to the Eyring equation, Eq. 5. Fitted parameters are listed in Table 1. **b** Temperature dependence of k_{non} and k_{cat}/K_m. Kinetic parameters were fitted to the Eyring equation, Eq. 5. Fitted parameters are listed in Table 1. **c** Energy profile for the hydrolysis of X2 on and off the enzyme at 25 °C

Most notable regarding the glycoside hydrolysis reactions off the enzyme are the high activation enthalpy values $(\Delta H^{\ddagger}) : (\Delta H^{\ddagger})^{4NPX} = (\Delta H^{\ddagger})^{X2} = 30.1\,\text{kcal/mol} > (\Delta H^{\ddagger})^{4NPA} = 26.7\,\text{kcal/mol}$ at 25 °C (Table 1). The high activation enthalpies, mirrored by the high Q_{10} values of 4.7 and 5.7, reflect the difficulty in hydrolyzing glycosidic bonds [25]. These are accompanied by low negative activation entropy values ($T\Delta S^{\ddagger}$) as might be expected for the hydrolysis reactions: $(T\Delta S^{\ddagger})^{4NPX} = -1.1\,\text{kcal/mol} > (T\Delta S^{\ddagger})^{X2} = -1.43\,\text{kcal/mol} > (T\Delta S^{\ddagger})^{4NPA} = -2.87\,\text{kcal/mol}$. Similar values for $\Delta H^{\ddagger}$ (30 kcal/mol) and more negative values for $T\Delta S^{\ddagger}$ (−7 kcal/mol) have been reported for the spontaneous hydrolysis of methyl glucopyranosides [25]. The two activation energies combine to provide activation free-energy values that dictate relative rates of spontaneous hydrolysis at 25 °C for 4NPA, 4NPX, and X2 of 1.00, 0.063, and 0.038, respectively. On the enzyme, k_{cat} rates have the opposite trend with relative rates of SXA-catalyzed hydrolysis at 25 °C for X2, 4NPX, and 4NPA of 1.00, 0.19, and 0.017. The difference between hydrolysis rates on and off the enzyme is best seen in the ratios of k_{cat}/k_{non} where the relative values for X2, 4NPX, and 4NPA are 1, 0.12, and 0.0064, respectively. Thus, SXA is more effective catalyzing hydrolysis of its natural substrate (X2) than the artificial substrates 4NPX and 4NPA. These relationships are seen in the free-energy profiles of the three hydrolysis reactions (Figs. 6, 7, and 8), which are qualitatively similar and diverge by the magnitude of the rate enhancements.

Rate enhancements (k_{cat}/k_{non}), which are typical in their enthalpic origin, increase with decreasing temperature for substrates X2, 4NPX, and 4NPA (Figs. 6, 7, and 8). Unlike certain enzymes (e.g., cytidine deaminase [24]) whose $\Delta H^{\ddagger}$ values for k_{cat}/K_m are small

Table 1 Parameters for hydrolysis of substrates on and off the enzyme at pH 5.3 and 25 °C.

Parameter	Rate or equilibrium constant	Q_{10} (20–30 °C)	$\Delta G°$ or $\Delta G^{\ddagger}$ (kcal/mol)	$\Delta H°$ or $\Delta H^{\ddagger}$ (kcal/mol)	$T\Delta S°$ or $T\Delta S^{\ddagger}$ (kcal/mol)
k_{non}^{4NPX}	$(8.26\pm0.17)\times10^{-11}\ s^{-1}$	5.69	31.2±0.4	30.1±0.3	−1.10±0.23
k_{cat}/K_m^{4NPX}	$(45.4\pm0.6)\times10^{3}\ s^{-1}\ M^{-1}$	2.12	11.1±1.0	12.7±0.7	1.56±0.73
k_{cat}^{4NPX}	$35.3\pm0.2\ s^{-1}$	3.42	15.4±0.5	21.1±0.3	5.72±0.33
$1K_m^{4NPX}$	$1{,}290\pm20\ M^{-1}$	0.64	−4.25±0.99	−8.40±0.70	−4.16±0.70
$1/K_{tx}^{4NPX}$	$(5.36\pm0.11)\times10^{14}\ M^{-1}$	0.39	−20.1±1.0	−17.4±0.7	2.66±0.73
k_{cat}/k_{non}^{4NPX}	$(4.27\pm0.01)\times10^{11}$				
$k_{non}^{xylobiose}$	$(5.04\pm0.07)\times10^{-11}\ s^{-1}$	5.69	31.5±0.3	30.1±0.2	−1.43 ±0.19
$k_{cat}/K_m^{xylobiose}$	$(85.6\pm6.4)\times10^{3}\ s^{-1}\ M^{-1}$	1.96	10.7±0.8	11.3±0.6	0.635±0.572
$k_{cat}^{xylobiose}$	$186\pm1\ s^{-1}$	2.37	14.3±0.6	14.6±0.4	0.276±0.459
$1/K_m^{xylobiose}$	$459\pm37\ M^{-1}$	0.86	−3.64±0.80	−3.28±0.56	0.358±0.569
$1/K_{tx}^{xylobiose}$	$(1.70\pm0.13)\times10^{15}\ M^{-1}$	0.36	−20.8±0.8	−18.7±0.6	2.07±0.57
$k_{cat}/k_{non}^{xylobiose}$	$(3.69\pm0.05)\times10^{12}$				
k_{non}^{4NPA}	$(1.31\pm0.03)\times10^{-9}\ s^{-1}$	4.69	29.6±0.6	26.7±0.5	−2.87±0.40
k_{cat}/K_m^{4NPA}	$3{,}450\pm70\ s^{-1}\ M^{-1}$	2.45	12.7±0.6	15.2±0.4	2.50±0.42
k_{cat}^{4NPA}	$3.09\pm0.03\ s^{-1}$	2.60	16.8±0.4	16.3±0.3	−0.435±0.280
$1/K_m^{4NPA}$	$1{,}120\pm30\ M^{-1}$	0.97	−4.11±0.86	−1.17±0.61	2.94±0.61
$1/K_{tx}^{4NPA}$	$(2.58\pm0.86)\times10^{12}\ M^{-1}$	0.54	−16.9±0.6	−11.5±0.4	5.36±0.42
k_{cat}/k_{non}^{4NPA}	$(2.36\pm0.06)\times10^{9}$				

Thermodynamic parameters were calculated using the data and fits of Figs. 5, 6, 7, and 8. $K_{TX} = K_m \times k_{non}/k_{cat}$. Rate and equilibrium constants at 25 °C were determined at 25 °C for reactions on the enzyme. Rate constants at 25 °C off the enzyme were determined by extrapolation of the values plotted in Figs. 6, 7, and 8. $\Delta G°$ and $\Delta G^{\ddagger}$ values were calculated from the relationship $\Delta G = \Delta H - T\Delta S$. When they are calculated from the rate and equilibrium constants, $\Delta G°$ and $\Delta G^{\ddagger}$ values are similar to those listed, but associated error values are much smaller

(~2 kcal/mol) and make k_{cat}/K_m nearly temperature independent, SXA-catalyzed hydrolyses of X2, 4NPX, and 4NPA have relatively large values for $\Delta H^{\ddagger}$ (>10 kcal/mol) for k_{cat}/K_m and substantial temperature dependencies (Table 1). The relatively large values for $\Delta H^{\ddagger}$ of k_{cat}/K_m are smaller than the $\Delta H^{\ddagger}$ of k_{non} for the three substrates, and, accordingly, transition-state affinities (K_{TX}) increase with decreasing temperature, which is consistent with the formation of electrostatic and H-bonding interactions in the transition state that are not formed in the Michaelis complex.

Ground-state binding of the three substrates by SXA, which have similar K_m values and similar $\Delta G°$ values, shows striking differences in $\Delta H°$ and $\Delta S°$ values at 25 °C. Differences in $\Delta H°$ are seen in the slopes of Fig. 5 and the $\Delta H°$ values of −8.4, −3.3, and −1.2 kcal/mol for 4NPX, X2, and 4NPA, respectively (Table 1). The trend is reversed for the $\Delta S°$ values to result in similar $\Delta G°$ values for the three substrates. Whereas 4NPX has decreased entropy ($T\Delta S°$=−4.16 kcal/mol) in its $1/K_m$ term, 4NPA shows increased entropy ($T\Delta S°$=2.9 kcal/mol), and X2 has little or no change in entropy ($T\Delta S°$=0.4±0.6 kcal/mol). Decreased entropy upon binding 4NPX to SXA is expected for bringing two molecules together. Increased entropy upon binding 4NPA to SXA suggests weak interactions within the Michaelis complex [24]. Differences are seen between the three substrates in their associated activation entropies for the k_{cat} term, proceeding from the Michaelis complex to the transition-state complex (Figs. 6, 7, and 8, Table 1). The activation entropies (as $T\Delta S^{\ddagger}$ values) are 5.7, −0.4, and 0.3 kcal/mol for 4NPX, 4NPA, and X2, respectively. Thus, $T\Delta S^{\ddagger}$ works in favor of

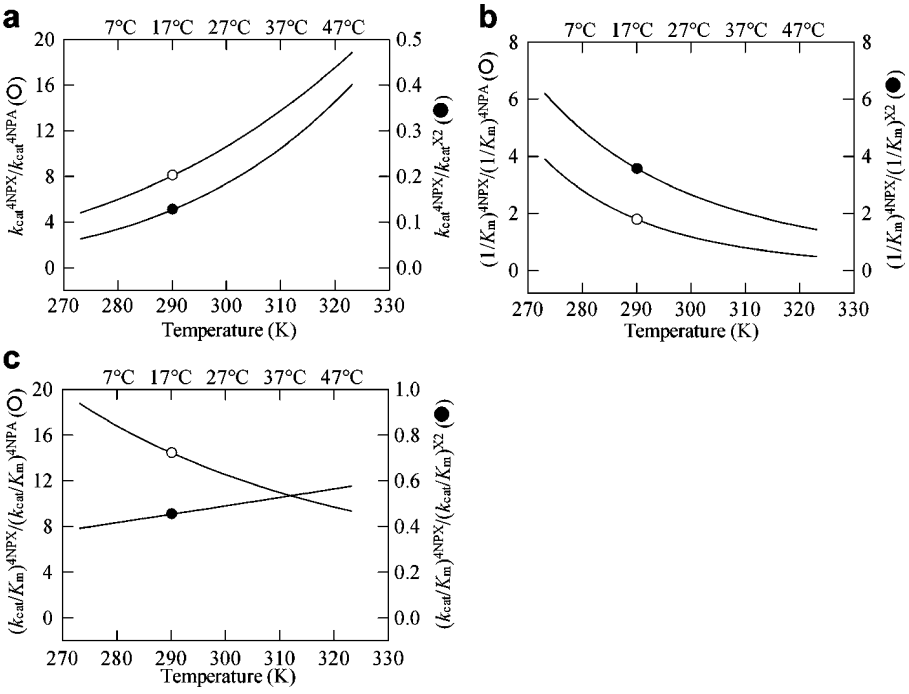

Fig. 9 Relative kinetic parameters for substrates of SXA-catalyzed hydrolysis reactions versus temperature. Kinetic parameters were determined at pH 5.3 and 5.5–40.4 °C. Data were fitted to Eqs. 4 and 5. The fitted parameters were used to calculate ratios of the parameters for two substrates versus temperature. **a** $k_{cat}^{4NPX}/k_{cat}^{4NPA}$ and $k_{cat}^{4NPX}/k_{cat}^{X2}$ versus temperature. **b** $(1/K_m)^{4NPX}/(1/K_m)^{4NPA}$ and $(1/K_m)^{4NPX}/(1/K_m)^{X2}$ versus temperature. **c** $(k_{cat}/K_m)^{4NPX}/(k_{cat}/K_m)^{4NPA}$ and $(k_{cat}/K_m)^{4NPX}/(k_{cat}/K_m)^{X2}$ versus temperature

substantially increased k_{cat}^{4NPX} and lower transition-state free-energy barrier for 4NPX. $T\Delta S^{\ddagger}$ has much less influence on 4NPA and X2 achieving transition states on the enzyme. Differences are apparent in the $T\Delta S^{\ddagger}$ and $\Delta H^{\ddagger}$ values that accompany binding of the respective transition states of the three substrates to free enzyme (Figs. 6, 7, and 8, Table 1). $\Delta H^{\ddagger}$ values for 4NPX (−17.4 kcal/mol) and X2 (−18.7 kcal/mol) are considerably higher than $\Delta H^{\ddagger}$ for 4NPA (−11.5 kcal/mol), reflecting weaker H-bonding and electrostatic interactions of $4NPA^{\ddagger}$ in binding to enzyme. $T\Delta S^{\ddagger}$ of 4NPA binding to enzyme (5.4 kcal/mol) is higher than the corresponding activation entropies of 4NPX (2.7 kcal/mol) and X2 (2.1 kcal/mol). If one assumes similar displacement of ordered water molecules from enzyme and substrate, the lower $T\Delta S^{\ddagger}$ of 4NPA may reflect greater mobility of $4NPA^{\ddagger}$ in the $ES^{\ddagger}$ complex.

Previously, we have shown that the ratio $(k_{cat}/K_m)^{4NPX}/(k_{cat}/K_m)^{4NPA}$ is nearly pH independent between pH 4.3 and pH 9.0, whereas $k_{cat}^{4NPX}/k_{cat}^{4NPA}$ and $1/K_m^{4NPX}/1/K_m^{4NPA}$ decrease with increasing pH in SXA-catalyzed reactions at 25 °C [7]. Figure 9 shows the temperature influence on the relative parameters at pH 5.3. $k_{cat}^{4NPX}/k_{cat}^{4NPA}$, $k_{cat}^{4NPX}/k_{cat}^{X2}$ and $(k_{cat}/K_m)^{4NPX}/(k_{cat}/K_m)^{X2}$ increase with increasing temperature, whereas $(k_{cat}/K_m)^{4NPX}/(k_{cat}/K_m)^{4NPA}$, $(1/K_m)^{4NPX}/(1/K_m)^{4NPA}$, and $(1/K_m)^{4NPX}/(1/K_m)^{X2}$ decrease with increasing temperature.

Off the enzyme, the mechanism yielding spontaneous rates calls for neighboring group participation from the C2–OH group addition to C1 with elimination of the aglycone. The addition product intermediate is subsequently hydrolyzed to yield the glycone. The two-step mechanism, which presumably occurs with retention of anomeric stereochemistry, does not operate on the enzyme, as the SXA-catalyzed hydrolysis of 4NPX and X2 have been characterized as proceeding with overall inversion of anomeric configuration through a single transition state [4]. Therefore, the mechanisms of hydrolysis off and on the enzyme are different and not ideal for comparisons. The k_{non} values reported here should be considered as upper limits for the rates of hydrolysis off the enzyme that occur through a mechanism similar to that which occurs on the enzyme. For example, the specific-acid- and specific-base-catalyzed rates at pH 5.3 (shown by the dotted lines of Fig. 4) have extrapolated k_{non} values of 1.5×10^{-6}, 1.5×10^{-5}, and 1.8×10^{-6} min^{-1} at 90 °C for 4NPX, 4NPA, and X2, respectively, which are 40-, 24-fold, and ninefold lower than the corresponding spontaneous rates and the relationship 4NPA > 4NPX > X2 is retained. Thus, our conclusions are not altered beyond the quantitative differences in k_{non}.

References

1. Henrissat, B. (1991). *The Biochemical Journal*, *280*, 309–316.
2. Henrissat, B., & Davies, G. J. (1997). *Current Opinion in Structural Biology*, *7*, 637–644. doi:10.1016/S0959-440X(97)80072-3.
3. Davies, G. J., & Sinnott, M. L. (2008). *The Biochemical Journal*, www.biochemj.org. doi:10.1042/BJ20080382.
4. Jordan, D. B., Li, X.-L., Dunlap, C. A., Whitehead, T. R., & Cotta, M. A. (2007). *Applied Biochemistry and Biotechnology*, *141*, 51–76. doi:10.1007/s12010-007-9210-8.
5. Jordan, D. B. (2008). *Applied Biochemistry and Biotechnology*, *146*, 137–149. doi:10.1007/s12010-007-8064-4.
6. Jordan, D. B., Li, X.-L., Dunlap, C. A., Whitehead, T. R., & Cotta, M. A. (2007). *Applied Biochemistry and Biotechnology*, *137–140*, 93–104. doi:10.1007/s12010-007-9042-6.
7. Jordan, D. B., & Li, X. L. (2007). *Biochimica et Biophysica Acta*, *1774*, 1192–1198.
8. Jordan, D. B., & Braker, J. D. (2007). *Archives of Biochemistry and Biophysics*, *465*, 231–246. doi:10.1016/j.abb.2007.05.016.

9. Saha, B. C. (2003). *Journal of Industrial Microbiology & Biotechnology*, *30*, 279–291. doi:10.1007/s10295-003-0049-x.
10. Gray, K. A., Zhao, L., & Emptage, M. (2006). *Current Opinion in Chemical Biology*, *10*, 141–146. doi:10.1016/j.cbpa.2006.02.035.
11. Shallom, D., & Shoham, Y. (2003). *Current Opinion in Microbiology*, *6*, 219–228. doi:10.1016/S1369-5274(03)00056-0.
12. Brunzelle, J. S., Jordan, D. B., McCaslin, D. R., Olczak, A., & Wawrzak, Z. (2008). *Archives of Biochemistry and Biophysics*, *474*, 157–166. doi:10.1016/j.abb.2008.03.007.
13. Whitehead, T. R., & Cotta, M. A. (2001). *Current Microbiology*, *43*, 293–298. doi:10.1007/s002840010304.
14. Gill, S. C., & von Hippel, P. H. (1989). *Analytical Biochemistry*, *182*, 319–326. doi:10.1016/0003-2697(89)90602-7.
15. Barshop, B. A., Wrenn, R. F., & Frieden, C. (1983). *Analytical Biochemistry*, *130*, 134–145. doi:10.1016/0003-2697(83)90660-7.
16. Kezdy, F. J., & Bender, M. L. (1962). *Biochemistry*, *1*, 1097–1106. doi:10.1021/bi00912a021.
17. McComb, R. B., Bond, L. W., Burnett, R. W., Keech, R. C., & Bowers Jr., G. N. (1976). *Clinical Chemistry*, *22*, 141–150.
18. Ziegenhorn, J., Senn, M., & Bücher, T. (1976). *Clinical Chemistry*, *22*, 151–160.
19. Jordan, D. B., Mertens, J. A., & Braker, J. D. (2008). *Biochimica et Biophysica Acta,* in press. doi:10.1016/j.bbapap.2008.09.015.
20. Leatherbarrow, R. J. (2001). *Grafit version 5*. Horley: Erithacus Software Ltd.
21. Harned, H. S., & Owen, B. O. (1958). *The physical chemistry of electrolytic solutions* (3rd ed.). New York: Reinhold.
22. Piszkiewicz, D., & Bruice, T. C. (1967). *Journal of the American Chemical Society*, *89*, 6237–6243. doi:10.1021/ja01000a044.
23. Larralde, R., Robertson, M. P., & Miller, S. L. (1995). *Proceedings of the National Academy of Sciences of the United States of America*, *92*, 8158–8160. doi:10.1073/pnas.92.18.8158.
24. Snider, M. J., Gaunitz, S., Ridgway, C., Short, S. A., & Wolfenden, R. (2000). *Biochemistry*, *39*, 9746–9753. doi:10.1021/bi000914y.
25. Wolfenden, R., Lu, X., & Young, G. (1998). *Journal of the American Chemical Society*, *120*, 6814–6815. doi:10.1021/ja9813055.